Microelectronics Reliability 98 (2019) 124–130

Contents lists available at ScienceDirect

Microelectronics Reliability

journal homepage: www.elsevier.com/locate/microrel

Bending reliability of flexible transparent electrode of gravure offset printed invisible silver-grid laminated with conductive polymer

Masato Ohsawa*, Natsuki Hashimoto

Institute for Super Materials, ULVAC, Inc., 5-9-6 Tohkohdai, Tsukuba, Ibaraki 300-2635, Japan

ARTICLE INFO

Keywords:
Ag nanoparticle
Flexible transparent electrode
Ag-grid
PEDOT:PSS
Gravure offset printing
Bending reliability

ABSTRACT

Invisible Ag-grid transparent electrodes at a line width of the Ag-grid of 5 μm and a line thickness of 0.6 μm have been prepared on a flexible polyethylene naphthalate (PEN) film substrate by a conventional gravure offset printing using our newly developed Ag nanoparticle ink. Furthermore, the Ag-grid electrodes were laminated with a poly(3,4-ethylenedioxythiophene): poly(styrenesulfonate) (PEDOT:PSS) layer. The bending flexibilities and repeated bending durabilities of the transparent electrodes have been investigated via bending tests. The Ag-grid laminated with PEDOT:PSS electrode shows no noticeable resistance change until the electrode is bended to an outer bending radius of 1.3 mm. Moreover, the Ag-grid laminated with PEDOT:PSS electrode shows no noticeable resistance change throughout the 10,000 outer bending cycles at a bending radius of 1.5 mm. The results show that the laminating with PEDOT:PSS enhances the bending reliability of the transparent electrodes.

1. Introduction

Transparent electrodes are indispensable components for optoelectronics devices, such as organic light emitting diodes [1], solar cells [2] and displays [3]. The conventional indium tin oxide (ITO) has been widely used as a transparent conductive electrode owing to excellent transmission and low sheet resistance. However, ITO is unfavorable in flexible electronic devices due to its intrinsic brittleness and high temperature treatment involved in its fabrication. To replace ITO, various alternative materials such as conductive polymers [4], carbon nanotubes [5,6], graphenes [7,8] and metal-grid electrodes [9–13] have been suggested as flexible transparent electrodes.

Among those alternative materials, metal-grid electrodes become very promising if printing technology enables the grid electrodes to be fabricated at lower cost since the printing technology helps improve the efficiency of material utilization as well as simplify the process steps for the fabrication of the grid electrodes. Recently, electrohydrodynamic (EHD) jet printing has received attention because of the potential for high resolution printing and has being studied [14–16]. Microcontact printing has also been reported to be useful for fabricating metal-grid transparent electrodes [17].

In this study, Ag-grid electrodes have been fabricated by a conventional gravure offset printing using our newly developed Ag nanoparticle ink based on our previous study [18]. The line width of the Ag-grid lines patterned by the printing in this study was 5 μm, which is beyond the pattern resolution capability of human eye [14]. Furthermore, the fabricated Ag-grid electrodes were laminated with a poly (3,4-ethylenedioxythiophene): poly(styrenesulfonate) (PEDOT:PSS) layer in this study. PEDOT:PSS is considered to be the most promising organic-based transparent electrode material and widely applied as an interfacial layer to improve hole injection in most organic devices [4,19,20]. The gravure offset printed Ag-grid laminated with PEDOT:PSS transparent electrodes have been reported to develop the excellent conductivity and transparency in our previous study. Our previous study demonstrated that the sheet resistance is down to 4 Ω/□ and the transmittance is up to 96% in the Ag-grid laminated with PEDOT:PSS electrodes by adjusting spacing between the grid lines [18].

In spite of invisible metal-grid electrodes are promising as flexible transparent electrodes, research on the bending reliability (bending flexibility and repeated bending durability) of the metal-grid electrodes is still limited. In terms of the practical realization of flexible electronic devices, the verification of the bending flexibility and repeated bending durability of the invisible metal-grid transparent electrode is substantially important.

In this study, bending flexibility and repeated bending durability of the Ag-grid laminated with PEDOT:PSS transparent electrode have been investigated via bending tests at a variety of bending radius and compared with those of the Ag-grid without PEDOT:PSS electrode and a commercial ITO transparent electrode.

* Corresponding author.
E-mail address: masato_oosawa@ulvac.com (M. Ohsawa).

https://doi.org/10.1016/j.microrel.2019.05.009
Received 21 February 2019; Received in revised form 9 April 2019; Accepted 13 May 2019
Available online 23 May 2019

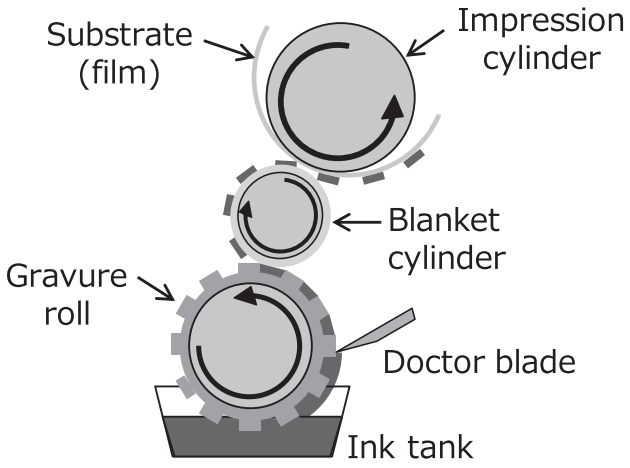

Fig. 1. A schematic illustration of gravure offset printing process.

2. Experimental method

2.1. Silver nanoparticle ink, printing and coating processes

Our newly developed ink (L-Ag Nano Metal Ink, ULVAC) involves Ag nanoparticles, the diameter of which is below 10 nm, stably dispersed in low-polar organic solvents. Dodecylbenzene was used as the solvent of the Ag nanoparticle ink in this study. The Ag nanoparticles went through the dispersing process in the solvent by a triple roll mill before printed. The viscosity of the prepared Ag ink was 2800 mPa·s. The content of the Ag nanoparticles in the ink was 70 wt%.

Fine Ag-grid electrodes were fabricated by a conventional gravure offset printing shown in our previous study [18]. Fig. 1 shows a schematic diagram of the gravure offset printing process. The fine grid electrode patterns to be printed are engraved on the gravure roll. In the gravure offset printing, ink from an ink tank is supplied into the whole surface of the gravure roll, and then the grooves on the gravure roll are filled with ink by a doctor blade. The process involves removing the excess ink using the doctor blade. The ink in the grooves is picked up by a polydimethylsiloxane (PDMS) rubber blanket cylinder. Control of the picked up ink layer on the PDMS rubber blanket cylinder is important to obtain desired patterns. Suitable PDMS is penetrated moderately by the ink in this study. Finally, the blanket cylinder is rotated over the target film substrate placed on the impression cylinder, thereby transferring the ink from the blanket cylinder to the substrate by a similar rotating action of the cylinders [21].

The developed Ag ink (L-Ag Nano Metal Ink, ULVAC) was applied to fabricate a fine invisible Ag-grid electrode pattern on a polyethylene naphthalate (PEN) film substrate (Teonex-Q65HA, TEIJIN), the thickness of which is 50 μm, by a gravure offset printing unit (K-PRINTING PROOFER, RK Print Coat Instruments). The printed area of the grid electrode patterns was 40 mm × 80 mm. The fabricated grid electrodes were annealed at 180 °C for 60 min. Then the Ag-grid electrode was over-coated with a conductive polymer poly (3, 4-ethylenedioxythiophene):poly (styrenesulfonate) (PEDOT:PSS) dispersion (composed of ARACOAT AS601D as the main agent and ARACOAT CL910 as the curing agent, Arakawa Chemical Industry) by an applicator (PI-1210, TESTER SANGYO) and cured at 100 °C for 1 min. The whole area of the fabricated Ag-grid electrode pattern was laminated with the PEDOT:PSS layer.

2.2. Characterization

The bending flexibilities and repeated bending durabilities of the fabricated electrodes of the Ag-grid laminated with and without PEDOT:PSS were evaluated by a bending endurance test machine (Tension-Free Folding Clamshell-type, YUASA SYSTEM). The electrode samples were bended in the bending angle range from 180° (flat state) to 0° at the prescribed bending radius. The repeated bending tests were carried out in the bending condition at a frequency of 0.5 Hz for 10,000 cycles. In the bending tests, the electrode samples were placed with the Ag-grid side outwards. The Ag-grid electrodes with the line width of 5 μm and spacing between the Ag-grid lines of 200 μm were used as the electrode samples in the bending tests. The sheet resistance values of the Ag-grid laminated with and without PEDOT:PSS electrodes are 4.9 Ω/□ and 6.1 Ω/□, respectively [18]. Electrical resistance changes of the fabricated electrodes were measured throughout the bending tests. The gauge length of the electrode sample loaded by bending, L_g is written with the following equation:

$$L_g = \pi r \quad (1)$$

where r is the bending radius of the electrode. The electrical resistance changes of the electrodes were evaluated in the areas corresponding to the gauge length, L_g.

Focused ion beam (FIB)-prepared cross-sections of the Ag-grid laminated with and without PEDOT:PSS electrodes were observed by a field emission scanning electron microscope (FE-SEM S-5500, Hitachi).

3. Results and discussion

3.1. Surface morphology of the Ag-grid laminated with PEDOT:PSS electrode

The fabricated Ag-grid electrode was over-coated with the PEDOT:PSS dispersion by an applicator in this study. Shown in Fig. 2 is a bright-field scanning transmission electron microscope (BF-STEM) image of an FIB-prepared cross section of the Ag-grid laminated with PEDOT:PSS electrode. The laminated PEDOT:PSS layer relieves the elevations formed by the thickness of the Ag-grid lines as shown in Fig. 2(a). Moreover, the laminated PEDOT:PSS layer fills to flatten the asperities of the Ag-grid surfaces as shown in Fig. 2(b). The relief of the

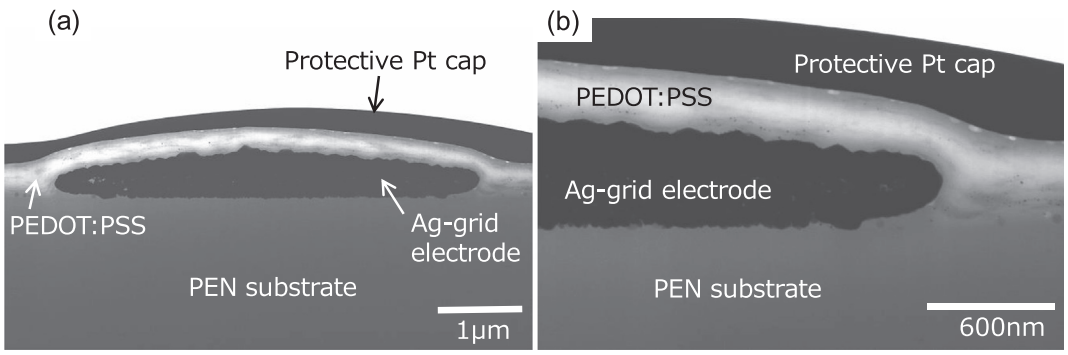

Fig. 2. FIB-prepared cross-sectional BF-STEM image of the Ag-grid laminated with PEDOT:PSS electrode: (a) low-magnification image, (b) high-magnification image.

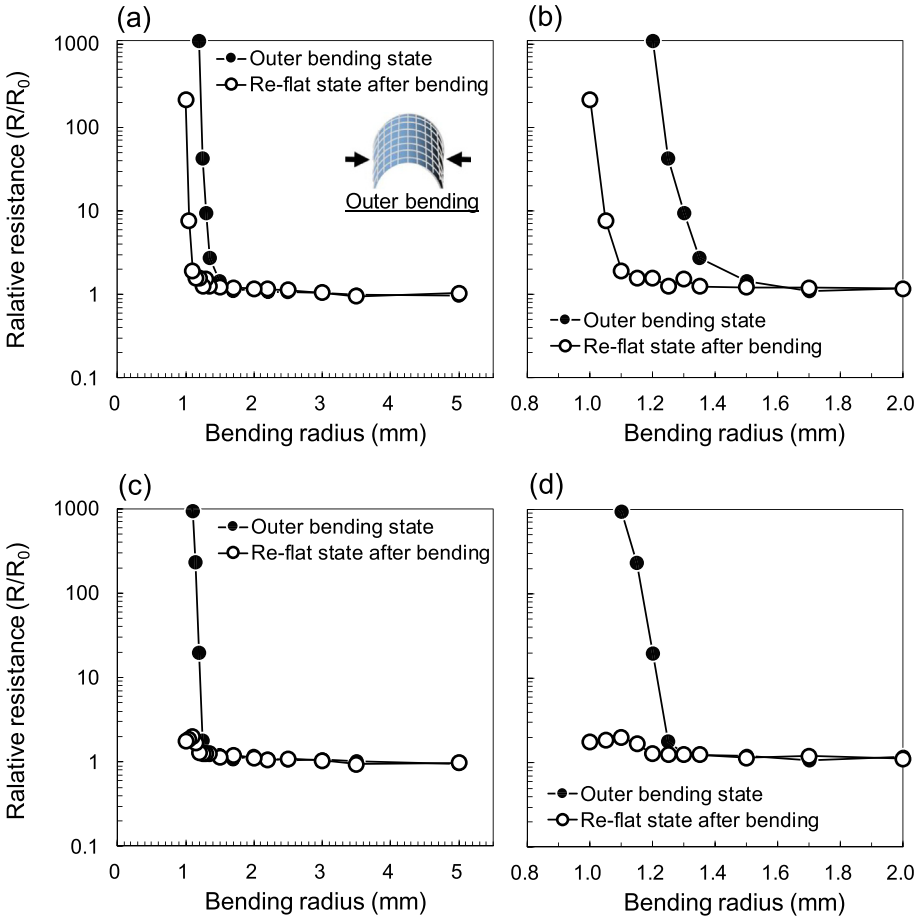

Fig. 3. Resistance of the Ag-grid laminated with and without PEDOT:PSS electrodes on the PEN film substrates measured in the outer bending state and the re-flat state after bending, normalized to the resistance measured in the initial flat state, as a function of outer bending radius. The inset in (a) shows the relationship between the direction of the Ag-grid lines and the bending direction. (a) Ag-grid electrode without PEDOT:PSS, (b) the detail with an enlarged scale of (a), (c) Ag-grid laminated with PEDOT:PSS electrode, (d) the detail with an enlarged scale of (c).

elevations and flattening of surfaces of the Ag-grids would be effective for depositing other thin films uniformly on the Ag-grid laminated with PEDOT:PSS transparent electrodes [18].

3.2. Outer bending flexibility at a variety of bending radius

Outer bending flexibilities of the Ag-grid laminated with and without PEDOT:PSS transparent electrodes have been evaluated at a variety of the bending radius. In the bending tests, the Ag-grid laminated with and without PEDOT:PSS electrodes were placed with the Ag-grid side outwards and subjected to tensile stress under the bending. The relationship between the direction of the Ag-grid lines and the bending direction is shown in the inset schematic illustration of Fig. 3(a). The change in resistance of the sample is expressed as R/R_0, where R_0 is the resistance of initial flat state and R is the resistance after bending at the prescribed bending radius. R was measured in both the bending state and the re-flat state after bending. Fig. 3 shows R/R_0 of the Ag-grid laminated with and without PEDOT:PSS electrodes as a function of bending radius.

As shown in Fig. 3(a),(b), in the Ag-grid without PEDOT:PSS electrode, R in the bending state almost remains unchanged until the sample is bended to an outer bending radius of 1.5 mm. R in the bending state increases sharply with decreasing bending radius in the bending radius range below 1.3 mm and reaches 1000 times as high as R_0 at an outer bending radius of 1.2 mm. R in the re-flat state after bending remains unchanged until the sample is bended to an outer bending radius of 1.1 mm. This indicates that recovery of the electrical resistance arises in the re-flat state after outer bending until the sample is bended to a bending radius of 1.1 mm. However, R in the re-flat state after bending increases sharply in the bending radius range below 1.1 mm and adequate recovery of the electrical resistance in the re-flat state does not arise in the bending radius range.

In the Ag-grid laminated with PEDOT:PSS electrode as shown in Fig. 3(c),(d), R in the bending state almost remains unchanged until the sample is bended to an outer bending radius of 1.3 mm. R in the bending state increases sharply with decreasing bending radius in the bending radius range below 1.2 mm and reaches 1000 times as high as R_0 at an outer bending radius of 1.1 mm. In contrast, R in the re-flat state after bending remains unchanged until the sample is bended to an outer bending radius of 1.0 mm. This indicates that recovery of the electrical resistance arises in the re-flat state after outer bending until the sample is bended to a bending radius of 1.0 mm.

The corresponding bending strain of the transparent electrode in this study has been calculated by the following equation [16,22,23]:

$$\text{Strain} = (h_f + h_s)/2r \approx h_s/2r \quad (2)$$

where, h_f, h_s and r denote the transparent electrode thickness, the substrate thickness and the bending radius, respectively. Fig. 4 shows R/R_0 of the Ag-grid laminated with and without PEDOT:PSS electrodes in the bending state and the re-flat state after bending as a function of bending strain. In the Ag-grid without PEDOT:PSS electrode, the recovery of electrical resistance in the re-flat state after bending does not arise adequately in the bending strain range above 2.3% (Fig. 4(a)). In contrast, the recovery of the electrical resistance arises adequately even in the bending strain range up to 2.5% in the Ag-grid laminated with PEDOT:PSS electrode (Fig. 4(b)). The Ag-grid laminated with PEDOT:PSS electrodes develop more superior bending flexibility compared to the Ag-grid without PEDOT:PSS electrodes. The superior bending flexibility is due to the lamination of PEDOT:PSS layer on the Ag-grid lines.

R of the invisible Ag-grid electrode shown in [16] has been reported to be 1.5 times R_0 at an outer bending strain of 2.1% in the bending

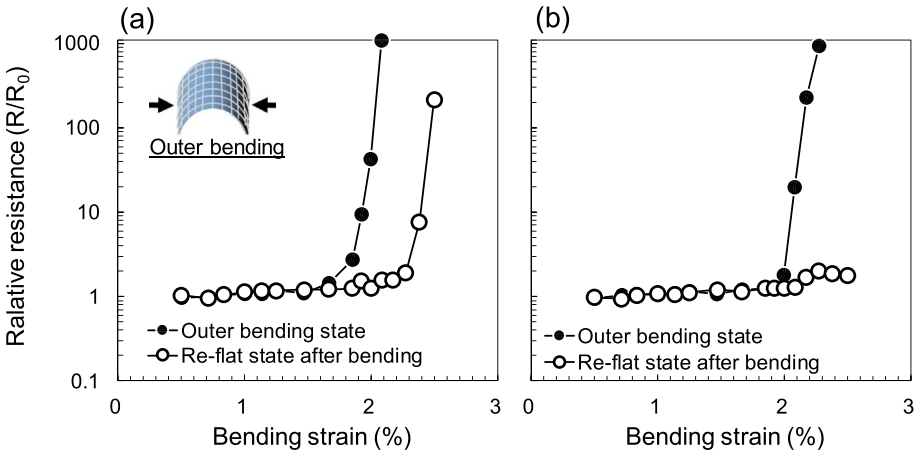

Fig. 4. Resistance of the Ag-grid laminated with and without PEDOT:PSS electrodes on the PEN film substrates measured in the outer bending state and the re-flat state after bending, normalized to the resistance measured in the initial flat state, as a function of outer bending strain. The inset in (a) shows the relationship between the direction of the Ag-grid lines and the bending direction. (a) Ag-grid electrode without PEDOT:PSS, (b) Ag-grid laminated with PEDOT:PSS electrode.

state. In contrast, R of the Ag-grid without PEDOT:PSS electrode in this study is 1000 times as high as R_0 at the same strain (Fig. 4(a)). R of the Ag-grid laminated with PEDOT:PSS electrode in this study is 20 times as high as R_0 at the same strain (Fig. 4(b)). This might be due to the difference of microstructure of the Ag-grid electrodes. The Ag ink used in [16] consisted of Ag nanoparticles with a mean diameter of about 300 nm and the obtained Ag-grid electrodes showed porous structure resulting from the grain boundaries of Ag nanoparticles. The porous structure might relax the bending strain. The Ag ink used in this study consists of Ag nanoparticles with a diameter below 10 nm. The fabricated Ag-grid electrodes in this study show more dense structure resulting from necking between the Ag nanoparticles and the grain growth by the annealing [18]. The more dense structure would be more sensitive to the bending strain.

A flexible transparent electrode of sputtered ITO/Ag/ITO multilayers has been reported in [24]. The resistance of the ITO/Ag/ITO transparent electrode increased with increasing outer bending strain in the strain range above 1.0%. The bending flexibilities of the Ag-grid laminated with and without PEDOT:PSS electrodes in this study are superior to the flexibility of the ITO/Ag/ITO electrode as shown in Fig. 4.

The outer bending flexibility of a commercial ITO on poly (ethylene terephthalate) (PET) film substrate has also been evaluated at a variety of the bending radius in this study. The sheet resistance, R_0 of the ITO and the thickness of the PET film substrate is 250 Ω/□ and 130 μm, respectively. Fig. 5 shows R/R_0 of the ITO electrode as a function of outer bending strain. The corresponding bending strain was also calculated in Eq. (2). R of the ITO electrode increases sharply with increasing bending strain in the bending strain range above 1.1%. R in the re-flat state after bending is substantially equivalent to that in the outer bending state and no recovery of the electrical resistance in the re-flat state after bending arises in the ITO electrode. This is due to the fact that ITO electrode is a ceramic-like oxide film and intrinsically brittle. As shown in Figs. 4(b) and 5, R of the Ag-grid laminated with PEDOT:PSS transparent electrode in the outer bending state remains unchanged in the bending strain range below 2.0%. The recovery of the electrical resistance in the re-flat state after bending arises adequately even in the bending strain range up to 2.5% in the Ag-grid laminated with PEDOT:PSS electrodes. The Ag-grid laminated with PEDOT:PSS transparent electrode develops excellent bending flexibility compared to the ITO transparent electrode.

3.3. Repeated outer bending durability

The repeated outer bending durabilities of the Ag-grid laminated with and without PEDOT:PSS transparent electrodes have been evaluated at a bending radius of 1.5 mm, which corresponds to an outer

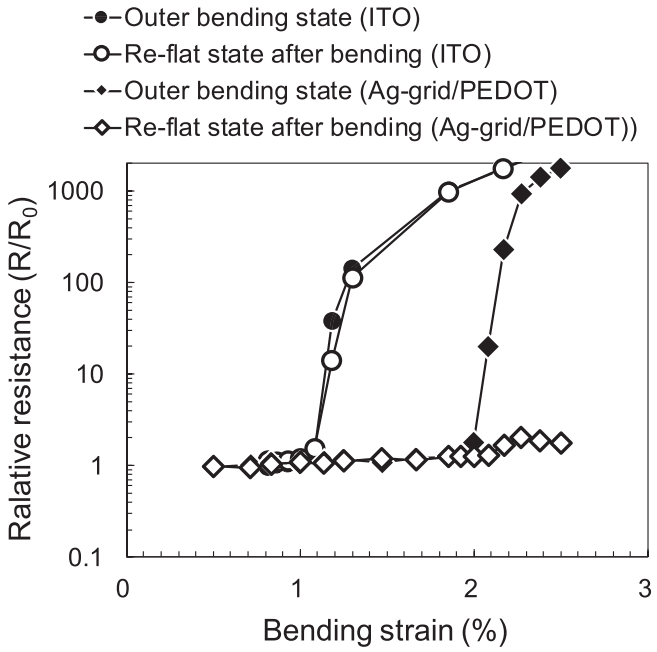

Fig. 5. Resistance of the commercial ITO electrode on the PET film substrate and the Ag-grid laminated with PEDOT:PSS electrode on the PEN film substrate measured in the outer bending state and the re-flat state after bending, normalized to the resistance measured in the initial flat state, as a function of outer bending strain.

bending strain of 1.7%. Fig. 6 shows R/R_0 in the re-flat state after bending of the Ag-grid laminated with and without PEDOT:PSS electrodes as a function of the bending cycles. In the Ag-grid without PEDOT:PSS electrode, R in the re-flat state after bending increases with increasing the number of bending cycle in the range above 100 cycles and reaches 1000 times higher than R_0 after the 10,000 bending cycles. In contrast, in the Ag-grid laminated with PEDOT:PSS electrode, R in the re-flat state after bending shows no noticeable change throughout the 10,000 bending cycles.

As shown in Eq. (2), bending strain increases with increasing substrate thickness at the same bending radius. The use of thinner substrate acts in favor of the bending reliability of electrodes on the substrate. It is also possible that invisible metal lines fabricated on transparent substrates are considered to be monolithic transparent electrodes. From the consideration, bending flexibility and repeated bending durability of the transparent electrodes are able to be evaluated regardless the thickness of substrates. In fact, some studies on the bending flexibility and durability of the electrodes have been reported without referring

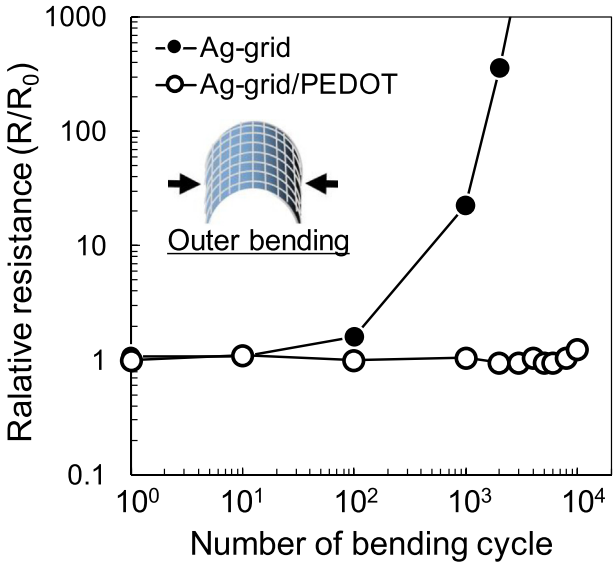

Fig. 6. Resistance of the Ag-grid laminated with and without PEDOT:PSS electrodes on the PEN film substrates measured in the re-flat state after bending, normalized to the resistance measured in the initial flat state, during repeated outer bending (bending at a radius of 1.5 mm). The inset shows the relationship between the direction of the Ag-grid lines and the bending direction.

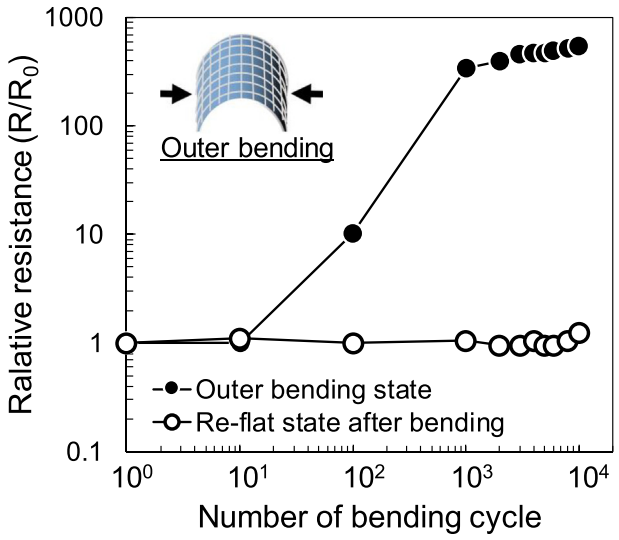

Fig. 7. Resistance of the Ag-grid laminated with PEDOT:PSS electrodes on the PEN film substrate measured in the bending state and re-flat state after the bending, normalized to the resistance measured in the initial flat state, during repeated outer bending (bending at a radius of 1.5 mm, which corresponds to a bending strain of 1.7%). The inset shows the relationship between the direction of the Ag-grid lines and the bending direction.

the thickness of substrates [4,25]. The bending flexibility and repeated bending durability of a transparent electrode of silver nanowire coated on a PDMS substrate (PDMS/AgNW) were reported without referring the thickness of substrate in [25]. R of the PDMS/AgNW increased with increasing outer bending cycles and reached 1.8 times R_0 after the 4000 outer bending cycles at a bending radius of 3 mm. In contrast, R of the Ag-grid laminated with PEDOT:PSS electrode in this study reaches only 1.2 times R_0 after the 10,000 outer bending cycles at a bending radius of 1.5 mm (Fig. 6). The bending durability of the Ag-grid laminated with PEDOT:PSS electrode on the PEN substrate in this study is superior to that of the PDMS/AgNW transparent electrode.

R/R_0 in the bending state of the Ag-grid laminated with PEDOT:PSS transparent electrode has also been evaluated throughout the 10,000 outer bending cycles at a bending radius of 1.5 mm, which corresponds to a bending strain of 1.7%. Fig. 7 shows R/R_0 in the bending state and the re-flat state after bending of the Ag-grid laminated with PEDOT:PSS transparent electrode as a function of the bending cycles. R in the bending state of the Ag-grid laminated with PEDOT:PSS electrode increases with increasing the bending cycles and reaches 600 times as high as R_0 after the 10,000 bending cycles. Notice that R in the re-flat state after bending shows no noticeable change throughout the 10,000 bending cycles. This indicates that adequate recovery of electrical resistance arises in the re-flat state after repeated outer bending at a radius of 1.5 mm.

Shown in Fig. 8 are scanning electron microscope (SEM) images of an FIB-prepared cross sections of the Ag-grid laminated with and without PEDOT:PSS electrodes after the 10,000 outer bending cycles at a bending radius of 1.5 mm. Intralaminar fracture propagation accompanied by horizontal cracks within the Ag-grid layer is clearly observed in the repeatedly bended Ag-grid without PEDOT:PSS electrode (Fig. 8(a),(b)). On the other hand, clear fractures and cracks are not observed although a horizontally connected-void layer within the Ag-grid layer is observed in the repeatedly bended Ag-grid laminated with PEDOT:PSS electrode (Fig. 8(c),(d)). The results show that the laminating with PEDOT:PSS enhances the repeated bending durability of the Ag-grid transparent electrode.

As shown in Fig. 3, the resistances of the Ag-grid laminated with and without PEDOT:PSS electrodes remain unchanged at a bending radius of 1.5 mm. However, the repeated bending test of the Ag-grid without PEDOT:PSS electrode at a bending radius of 1.5 mm shows a significant increase in the resistance throughout 10,000 bending cycles as shown in Fig. 6. The results exhibit that the damage of the Ag-grid caused by severe bending strain cycles is accumulated throughout the bending cycles and brings increase of the resistance. The Ag-grid electrodes fabricated by the Ag nanoparticle ink in this study have a structure attributed to sintering with necking between the Ag nanoparticles and grain growth by the annealing. The sintering with necking between the Ag nanoparticles and grain growth generate fine voids in grain boundaries of the Ag-grid layer. Therefore, the fine voids pre-exist in the Ag-grid electrodes as shown in our previous study [18]. The pre-existing fine voids would be the initiation of the horizontal cracks within the Ag-grid layer shown in Fig. 8(a). The intralaminar fracture propagation accompanied by horizontal cracks within the Ag-grid layer would be due to the crack growth which proceeds so as to connect the neighboring pre-existing fine voids. The horizontal crack cleavage would cause critical vertical cracks throughout the severe repeated bending strain (Fig. 8(b)). Meanwhile, the repeated bending test of the Ag-grid laminated with PEDOT:PSS electrode at a bending radius of 1.5 mm does not show a significant increase in the resistance throughout 10,000 bending cycles as shown in Fig. 6. As shown in Fig. 8(c),(d), the Ag-grid laminated with PEDOT:PSS electrode after the 10,000 bending cycles does not exhibit the critical crack cleavage although exhibits a connected-void layer in the Ag-grid layer. The connected-void layer would indicate the initial state of crack growth which proceeds so as to connect the neighboring pre-existing fine voids. The lamination with PEDOT:PSS would suppress the crack growth and critical crack cleavage. The PEDOT:PSS dispersion used in this study contains small amount of polymeric binder. Therefore, the PEDOT:PSS layer would suppress the bending strain and contribute to the recovery of resistance in the re-flat state after bending shown in Fig. 7. A fine void space is observed in the PEDOT:PSS layer around the interface between the PEDOT:PSS layer and Ag-grid layer shown in Fig. 8(d). The void space would be yielded by stretching of the PEDOT:PSS layer throughout the bending cycles.

The repeated outer bending durability of the mentioned above commercial ITO electrode on PET substrate has also been evaluated at a bending radius of 3.85 mm, which corresponds to a bending strain of

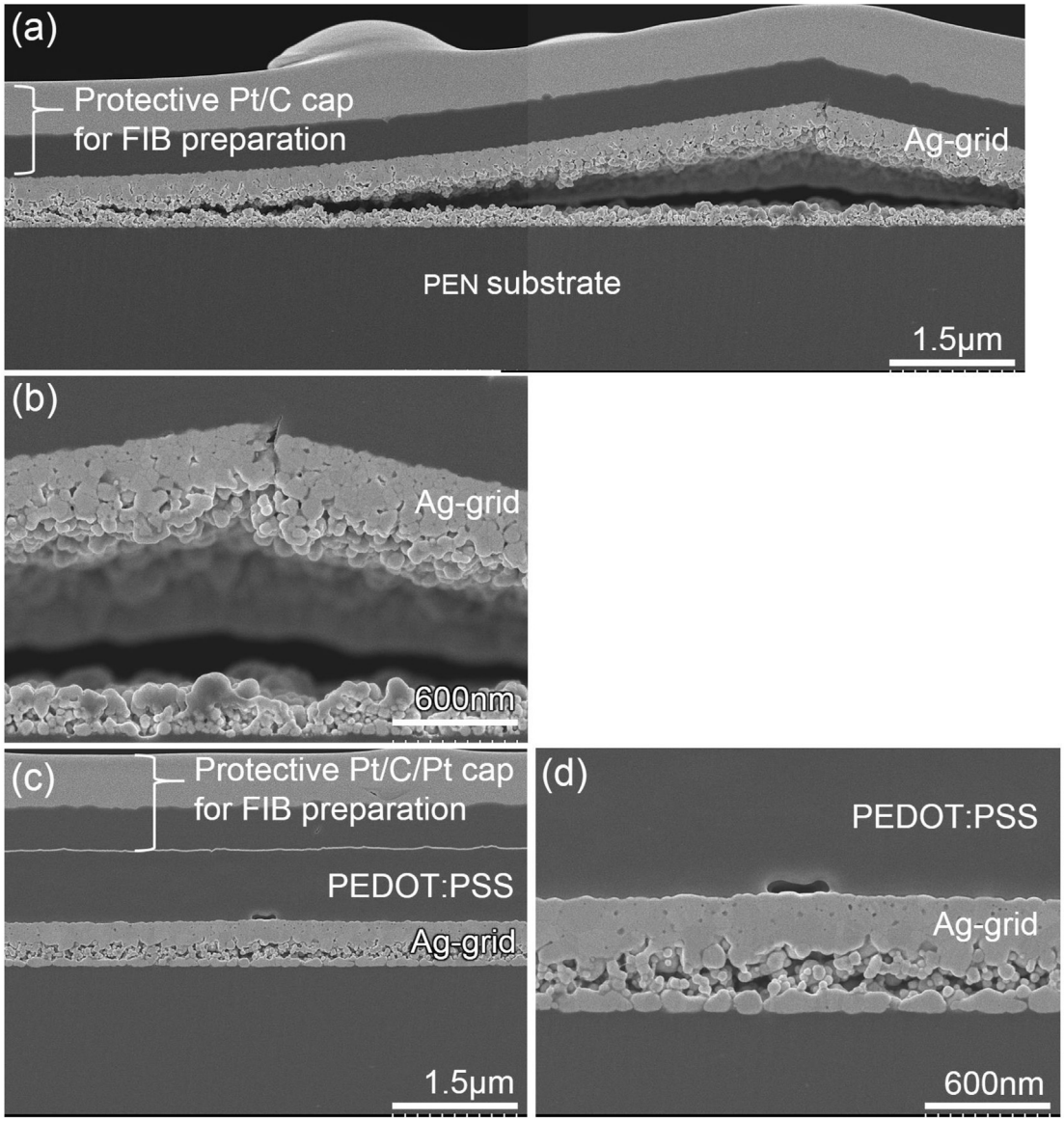

Fig. 8. FIB-prepared cross-sectional SEM images of the Ag-grid without PEDOT:PSS electrode: (a) low-magnification image, (b) high-magnification image, and of the Ag-grid laminated with PEDOT:PSS electrode: (c) low-magnification image, (b) high-magnification image, after the 10,000 outer bending cycles at a bending radius of 1.5 mm.

1.7%. Fig. 9 shows R/R_0 in the bending state and the re-flat state after bending of the ITO electrode as a function of outer bending cycles at a bending strain of 1.7%. R of the ITO electrode increases notably by one bending cycle both in the bending state and the re-flat state after bending and reaches 2000 times as high as R_0 after the 10,000 bending cycles. R in the re-flat state after bending is substantially equivalent to that in the outer bending state and no recovery of the electrical resistance in the re-flat state after bending arises in the ITO electrode. This is due to the fact that ITO electrode is a ceramic-like oxide film and intrinsically brittle. The Ag-grid laminated with PEDOT:PSS transparent electrodes develop excellent repeated bending durability compared to the ITO transparent electrode.

An assumption of a perfect plastic deformation in which the resistivity and the total volume of an electrode remain constant gives the following equation to estimate the geometric contribution to the resistance increase:

$$R/R_0 = (L/L_0)^2 = (1 + \varepsilon)^2 \quad (3)$$

where L_0 is the original electrode length, and L is the deformed electrode length ($L / L_0 = 1 + \varepsilon$, where ε is the strain) [26,27]. The sharp increases of R/R_0 shown in Figs. 4 and 7 are too high to explain by the perfect plastic deformation given in Eq. (3). Therefore, the sharp increases of R/R_0 in the Ag-grid laminated with and without PEDOT:PSS electrodes would be due to the crack disconnection of the Ag-grid caused by the bending. The adequate recovery of the electrical resistance of the Ag-grid laminated with PEDOT:PSS electrodes in the re-flat state after bending shown in Figs. 4(b) and 7 may be due to the PEDOT:PSS layer shrinkage and closure of the cracks in the Ag-grid caused by re-flattening after the outer bending. A compressive stress arises in the re-flat Ag-grid layer if the elastic strain of the PEDOT:PSS layer is much higher than that of the Ag-grid layer. The compressive stress might close the cracks in the Ag-grid layer. The conductivity of the PEDOT:PSS layer would also assist the conductivity of the cracked Ag-grid layer.

4. Conclusion

In this paper, invisible Ag-grid transparent electrodes at a line width

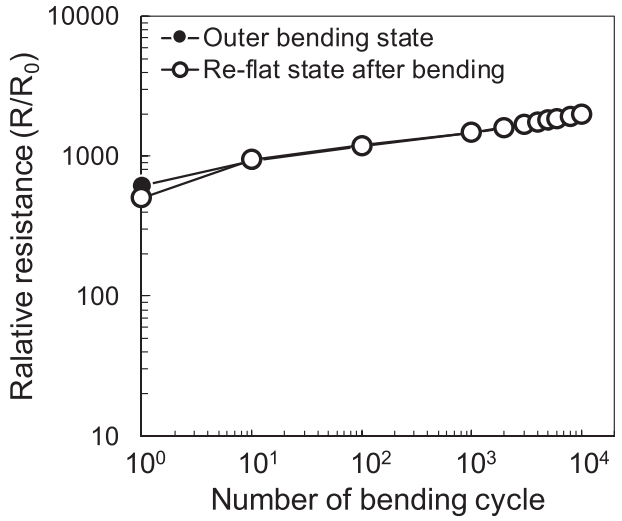

Fig. 9. Resistance of the commercial ITO transparent electrode on the PET film substrate measured in the bending state and re-flat state after the bending, normalized to the resistance measured in the initial flat state, during repeated outer bending (bending at a radius of 3.85 mm, which corresponds to a bending strain of 1.7%).

of the Ag-grid of 5 μm and a line thickness of 0.6 μm have been prepared on a flexible PEN film substrate by a conventional gravure offset printing using our newly developed Ag nanoparticle ink. Furthermore, the Ag-grid electrodes were laminated with a PEDOT:PSS layer. The bending flexibilities and repeated bending durabilities of the transparent electrodes have been investigated via bending tests. The Ag-grid laminated with PEDOT:PSS electrode shows no noticeable resistance change until the electrode is bended to an outer bending radius of 1.3 mm. Moreover, the Ag-grid laminated with PEDOT:PSS electrode shows no noticeable resistance change throughout the 10,000 outer bending cycles at a bending radius of 1.5 mm in the re-flat state after bending. The results show that the laminating with PEDOT:PSS enhances the bending reliability (bending flexibility and repeated bending durability) of the transparent electrodes. It seems that the enhanced bending reliability is due to the suppression of crack cleavage in the Ag-grid and the assistance of conductivity by laminating with the PEDOT:PSS layer. The bending reliability of the Ag-grid laminated with PEDOT:PSS transparent electrode is superior to that of an ITO transparent electrode. The Ag-grid laminated with PEDOT:PSS electrodes would have potential applications as flexible transparent electrodes for bendable optoelectronic devices.

Acknowledgements

The PEDOT:PSS dispersion in this work was provided by Arakawa Chemical Industry, Ltd. Fruitful discussions with Mr. K. Kajita at Arakawa Chemical Industry Ltd. are greatly appreciated.

References

[1] C.W. Joo, J. Lee, W.J. Sung, J. Moon, N.S. Cho, H.Y. Chu, J.I. Lee, ITO/metal/ITO anode for efficient transparent white organic light-emitting diodes, Jpn. J. Appl. Phys. 54 (2015) 02BC04.
[2] J. Wu, H.A. Becerril, Z. Bao, Z. Liu, Y. Chen, P. Peumans, Organic solar cells with solution-processed graphene transparent electrodes, Appl. Phys. Lett. 92 (2008) 263302.
[3] S.K. Park, J.I. Han, W.K. Kim, M.G. Kwak, Deposition of indium–tin-oxide films on polymer substrates for application in plastic-based flat panel displays, Thin Solid Films 397 (2001) 49–55.
[4] S.I. Na, S.S. Kim, J. Jo, D.Y. Kim, Efficient and flexible ITO-free organic solar cells using highly conductive polymer anodes, Adv. Mater. 20 (2008) 4061–4067.
[5] Z. Wu, Z. Chen, X. Du, J.M. Logan, J. Sippel, M. Nikolou, K. Kamaras, J.R. Reynolds, D.B. Tanner, A.F. Hebard, A.G. Rinzler, Transparent, conductive carbon nanotube films, Science 305 (2004) 1273–1276.
[6] V. Sharma, S. Singh, P. Garg, K. Asokan, K. Sachdev, Enhanced electrical conductivity in Xe ion irradiated CNT based transparent conducting electrode on PET substrate, Mater. Res. Express 5 (2018) 025037.
[7] X. Wang, L. Zhi, K. Müllen, Transparent, conductive graphene electrodes for dye-sensitized solar cells, Nano Lett. 8 (2008) 323–327.
[8] I. Banerjee, S.K. Mahapatra, C. Pal, A.K. Sharma, A.K. Ray, Effect of plasma power on reduction of printable graphene oxide thin films on flexible substrates, Mater. Res. Express 5 (2018) 056405.
[9] M.G. Kang, M.S. Kim, J. Kim, L.J. Guo, Organic solar cells using nanoimprinted transparent metal electrodes, Adv. Mater. 20 (2008) 4408–4413.
[10] J. Zou, H.L. Yip, S.K. Hau, A.K.Y. Jen, Metal grid/conducting polymer hybrid transparent electrode for inverted polymer solar cells, Appl. Phys. Lett. 96 (2010) 203301.
[11] P. Yi, C. Zhang, L. Peng, X. Lai, Flexible silver-mesh electrodes with moth-eye nanostructures for transmittance enhancement by double-sided roll-to-roll nanoimprint lithography, RSC Adv. 7 (2017) 48835–48840.
[12] Y. Galagan, J.E.J. Rubingh, R. Andriessen, C.C. Fan, P.W. Blom, S.C. Veenstra, J.M. Kroon, ITO-free flexible organic solar cells with printed current collecting grids, Sol. Energy Mater. Sol. Cells 95 (2011) 1339–1343.
[13] C. Zhu, R. Tan, W. Song, B. Ouyang, M. Cai, S. Zhoul, Y. Lu, N. Li, A cracked polymer templated Ag network for flexible transparent electrodes and heaters, Mater. Res. Express 5 (2018) 066427.
[14] Y. Jang, J. Kim, D. Byun, Invisible metal-grid transparent electrode prepared by electrohydrodynamic (EHD) jet printing, J. Phys. D. Appl. Phys. 46 (2013) 155103.
[15] C. Yang, J. Kim, Embedding of inkjet-printed Ag-grid/ITO hybrid transparent electrode into a plastic substrate for flexible electronic devices, Bull. Mater. Sci. 41 (2018) 3.
[16] S.M. Yang, Y.S. Lee, Y. Jang, D. Byun, S.H. Choa, Electromechanical reliability of a flexible metal-grid transparent electrode prepared by electrohydrodynamic (EHD) jet printing, Microelectron. Reliab. 65 (2016) 151–159.
[17] Z. Xin, Y. Liu, X. Li, S. Liu, Y. Fang, Y. Deng, C. Bao, L. Li, Conductive grid patterns prepared by microcontact printing silver nanoparticles ink, Mater. Res. Express 4 (2017) 015021.
[18] M. Ohsawa, N. Hashimoto, Flexible transparent electrode of gravure offset printed invisible silver-grid laminated with conductive polymer, Mater. Res. Express 5 (2018) 085030.
[19] M. Glatthaar, M. Niggemann, B. Zimmermann, P. Lewer, M. Riede, A. Hinsch, J. Luther, Organic solar cells using inverted layer sequence, Thin Solid Films 491 (2005) 298–300.
[20] T. Aernouts, P. Vanlaeke, W. Geens, J. Poortmans, P. Heremans, S. Borghs, R. Mertens, R. Andriessen, L. Leenders, Printable anodes for flexible organic solar cell modules, Thin Solid Films 451 (2004) 22–25.
[21] W.X. Huang, S.H. Lee, H.J. Sung, T.M. Lee, D.S. Kim, Simulation of liquid transfer between separating walls for modeling micro-gravure-offset printing, Int. J. Heat Fluid Flow 29 (2008) 1436–1446.
[22] Z. Suo, E.Y. Ma, H. Glescova, S. Wanger, Mechanics of rollable and foldable film-on-foil electronics, Appl. Phys. Lett. 74 (1999) 1177–1179.
[23] T. Sekitani, Y. Kato, S. Iba, H. Shinaoka, T. Someya, T. Sakurai, S. Takagi, Bending experiment on pentacene field-effect transistors on plastic films, Appl. Phys. Lett. 86 (2005) 073511.
[24] T.H. Kim, S.H. Park, D.H. Kim, Y.C. Nah, H.K. Kim, Roll-to-roll sputtered ITO/Ag/ITO multilayers for highly transparent and flexible electrochromic applications, Sol. Energy Mater. Sol. Cells 160 (2017) 203–210.
[25] X. Liang, T. Zhao, P. Zhu, Y. Hu, R. Sun, C.P. Wong, Room-temperature nanowelding of a silver nanowire network triggered by hydrogen chloride vapor for flexible transparent conductive films, ACS Appl. Mater. Interfaces 9 (2017) 40857–40867.
[26] N. Lu, Z. Suo, J.J. Vlassak, The effect of film thickness on the failure strain of polymer-supported metal films, Acta Mater. 58 (2010) 1679–1687.
[27] O. Glushko, V.M. Marx, C. Kirchlechner, I. Zizak, M.J. Cordill, Recovery of electrical resistance in copper films on polyethylene terephthalate subjected to a tensile strain, Thin Solid Films 552 (2014) 141–145.